Simulation and experimental validation of resonant electric markers used for medical device tracking in magnetic resonance imaging

Johannes Krug, Karl Will and Georg Rose

***Abstract*— Magnetic resonance imaging (MRI), which was traditionally used for patient diagnosis, has gained in importance in minimally invasive interventions in the recent past. Hence, there is an increasing demand for medical devices compatible with the MR environment. One of the challenges is to visualize the medical devices, e.g. catheters, within the MR image. Several methods exist to cope with this task.**

The approach of this work uses resonant electric circuits as markers visible within the MR image. The markers are fabricated using a sophisticated micro systems technology process. The self-sufficient resonant markers are placed at the tip of 6 F catheters.

Different simulations of the resonant marker's magnetic field distribution within the high frequency magnetic field are performed. These simulation results are validated with the findings from our experimental measurements and will be used for the further development and improvement of the resonant electric markers.

I. INTRODUCTION

The most common application of magnetic resonance imaging in the past was in diagnostics. But with the recent development of MRI scanners offering open bores that allow a better access to the patient as well as fluoroscopic imaging functionalities, MRI has gained high interest in therapeutic applications in the last couple of years.

Catheters are used in many applications of minimal invasive interventions. However, due to the materials used to manufacture the catheters, they either generate strong artifacts or they are not visible within the MR image. To visualize and track the catheter in the MR image, different methods have been proposed. These methods can be divided into three groups: active, semi-active and passive tracking methods [1]. One *active* method is to generate a local magnetic field inhomogeneity with a DC current in a miniature coil [2], [3]. Another active approach is to locally acquire three 1-D projections with a receiver coil placed at the tip of a catheter to determine the position of the medical device [4]. The *semi-active* approach covers resonant electric circuits placed on the catheter's tip to provide a local gain of the B_1 field used for spin excitation [5]. These resonant electric circuits are assembled using a capacitor (C) and a coil (L) with its intrinsic series resistance (R_S). In addition to the stand alone resonant electric circuit, an optical method was proposed to detune the resonant electric circuit using a PIN-photodiode that manipulates the circuit's total capacitance [6]. *Passive* approaches modify the magnetic susceptibility properties of the catheter's material to cause local field inhomogeneities leading to signal voids [7].

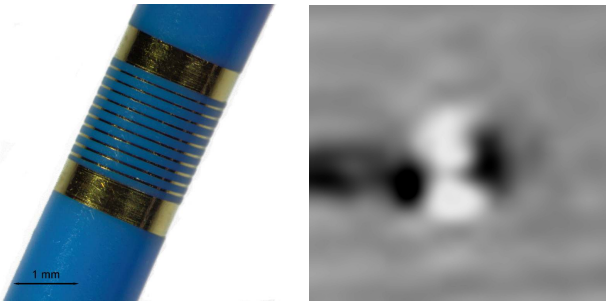

(a) Coil of the resonant electric marker on a catheter's tip

(b) MR image of (a)

Fig. 1. Manufactured resonant electric circuit and its visibility within the MR image

This paper describes the simulation of the resonant electric circuits used for semi-active tracking approaches. The resonant structures are fabricated using a micro systems technology developed by our group [8]. Practical measurements using these manufactured markers are compared to the simulation results. The effects observed during measurements are verified by simulations. These simulations are required for the further analysis of the resonant electric marker's behavior.

II. MATERIAL AND METHODS

A. Manufacturing the resonant electric markers

The coil of the resonant circuit is fabricated using an aerosol deposition process [8]. This process is applied to the cylindrical structure of the catheter. A discrete surface mount device is used as capacitor in the current design. The catheter with the resonant structure can be seen in Fig. 1(a). The fabrication process allows for a precise tuning of the coil's inductance to the desired resonant frequency of the circuit. Hence, additional tuning methods are not required.

B. Experimental measurements in an open MR tomograph

The catheter loaded with the resonant marker is placed in a phantom with T1/T2 properties of muscle tissue. The experiments were performed in an open MR scanner (Philips Panorama, 1 T). For a magnetic flux density of 1 T for the static B_0 field, the frequency for the rotating B_1 field is 42.57 MHz. A T1-FFE image sequence is used for the experimental measurements. The same sequence is also used for the image guided interventions, e.g liver biopsies [9]. A wide range of flip angles from 1° to 90° has been applied

This research was founded by the Federal Ministry of Education and Research (BMBF) in context of the Innoprofile 'INKA' project.

J. Krug, K. Will and G. Rose are with the Chair for Healthcare Telematics and Medical Engineering, University of Magdeburg, 39106 Magdeburg, Germany (Johannes.Krug@ovgu.de)

to study the effects of different B_1 fields on the resonant structure and its resulting interaction with the surrounding material of the phantom. The local B_1 field amplification of the resonant electric circuit is visible within the MR image as shown in Fig. 1(b) and is explained in section II-C.

C. Theory of MR signals and resonant circuits

For a given main magnetic field $|B_0| = 1\,\mathrm{T}$ and a gyromagnetic ratio $\gamma/2\pi = 42.576\,\mathrm{MHz/T}$ for hydrogen protons (^{1}H), the Lamor frequency is $f_0 = 42.576\,\mathrm{MHz}$. The precession axis of the ^{1}H protons is aligned (anti-)parallel to the $\vec{B_0}$ field. To put the longitudinal magnetization into the plane perpendicular to $\vec{B_0}$, a second magnetic field, B_1, rotates perpendicular to $\vec{B_0}$ with the given Lamor frequency. The gyroscopic rotation of the net magnetization is in case of on-resonance excitation $\omega_{rot} = \gamma B_1$. The desired flip angle α is determined by the duration T and by the intensity $|B_1|$ of the applied electromagnetic pulse:

$$\alpha = \gamma B_1 T \tag{1}$$

The signal induced in the receiver coil is caused by relaxation effects of the net magnetization, whereas its intensity depends on the previous applied flip angle. Therefore, the aim of using resonant markers is to locally increase the flip angle α by locally increasing the B_1 field.

The resonant marker can be modeled as a parallel $R_S LC$ circuit, where R_S and L are a series element parallel to C. The resulting magnetic flux density ϕ_{Res} of the resonant marker can be calculated as

$$\phi_{Res} = \phi_{Ext}(1 - jQ) \tag{2}$$

where ϕ_{Ext} is the magnetic flux from B_1 field and Q the quality factor of the resonant circuit. The Q factor is defined as $Q = \omega_0 L/R_S$ where ω_0 is the circuit's resonant frequency.

III. Simulation

A. Generating the rotating B_1 field

The rotating B_1 field used for spin excitation in the MR scanner can be generated by a birdcage coil. Therefore, a birdcage coil is constructed in the simulation environment in the first step. The complex geometry of the birdcage coil is simplified in a second step. All simulations are performed using the simulation software Microwave Studio from CST.

The birdcage coil resonator consists of eight cylindrical legs and is built as a low pass type as shown in Fig. 2(a). The *Java Birdcage Builder* (CNMRR, Penn State College) is used to calculate the capacitances. A vector plot of the simulated B_1 field distribution in the center plane of the coil at a fixed time point is shown in Fig. 2(b).

Compared to the size of the resonant electric circuit with a coil length of 2.6 mm and a coil radius of 1 mm, the dimensions of typical birdcage resonators are at least of a factor 100 of that of the resonant circuit.

To adjust the simulation volume to the dimension of the resonant electric circuit, a simplified model to generate the rotating B_1 field has to be used. The birdcage coil is replaced

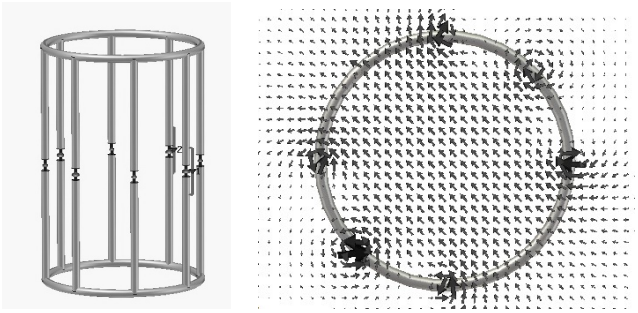

(a) Birdcage coil model (b) Vector plot of the H-field

Fig. 2. Simulation of the magnetic field distribution within a birdcage coil. Birdcage coil radius is 15 cm, length is 40 cm.

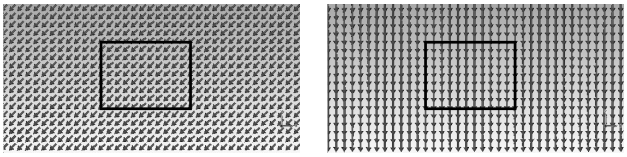

(a) Distribution 1 (b) Distribution 2

Fig. 3. Quantitative distribution of the rotating magnetic field vectors in two different points in time using the simplified excitation coil model (where the rectangle represents the outer dimensions of the resonant electric circuit ($2.6 \times 2\,\mathrm{mm}^2$)

by two perpendicular, rectangular coils driven by currents shifted 90° in phase. The resulting B_1 field distribution of this arrangement is given as a vector plot in Fig. 3.

The qualitative distribution of the magnetic field within the birdcage coil and the simplified rectangular coil is comparable within the region of interest. Here, both coil setups have a homogeneous field distribution. By using the simplified excitation model, the simulation time can be reduced due to the decrease of the simulated volume and the plain geometry of the excitation coils.

B. Simulation of the resonant electric circuit

The simulated resonant structure consists of a coil model with geometric dimensions similar to the fabricated coil. A lumped capacitive element is connected to the coil model as shown in Fig. 4(a). To change the Q factor of the resonant circuit, a lumped resistance in series to the coil is used.

The inductance of the coil can be calculated using the approximation equation for short coils:

$$L_{short} = N^2 \cdot \frac{\mu_0 \mu_r \pi r^2}{l + 0.909r} \tag{3}$$

which results in an inductance of 189 nH for the used dimensions (number of windings N=13, length of the coil l=2.6 mm and coil radius r=1 mm). The resulting theoretical capacitance for a resonant frequency of 42.57 MHz is 73 pF. This value is used for the lumped capacitor in the simulation.

Since an approximation formula is used to determine the capacitance, the resonance behavior is examined in the simulation environment by measuring the input port voltage reflection coefficient S_{11} of the resoant circuit as shown in Fig. 4(b). The simulated resonant frequency lies at 46.9 MHz.

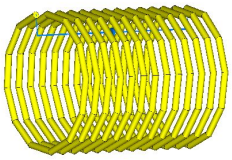

(a) 3D model of resonant marker

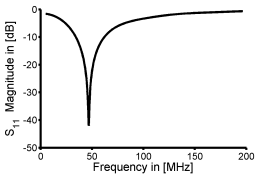

(b) Simulated frequency response of resonant marker

Fig. 4. Model of the resonant marker with the lumped capacitor element inside the coil. The frequency response is calculated using the S_{11} parameters.

This corresponds to an inductance of 155 nH for the simulated model. To tune the resonant electric circuit to the Lamor frequency of 42.57 MHz, a capacitance of 90 nF is used for the further simulations. Compared to these simulated values, the inductance of the manufactured coil is 170 nH.

The important information of the transient interaction between the external B_1 field and the field from the resonant marker is expected to be seen in the time domain. Therefore, the simulation is performed in the time domain using two different signals for the generation of the B_1 field. A sine function is used to reach a steady state of the markers field. Additionally, a sinc shaped signal is used to generate a more realistic B_1 excitation field. The simulation duration for each excitation signal setup was 400 ns with an excitation frequency of 42.57 MHz.

The rotating B_1 field generates an alternating field vector through the coil of the resonant marker. Since the marker is tuned to the frequency of the B_1 field, the magnetic field within and around the resonant marker is increasing with every period of excitation due to the storage of energy within the resonant electric circuit. The maximum value of the magnetic field within the resonant marker depends on the marker's Q-factor and its orientation related to the B_1 field. A higher Q-factor of the resonant electric circuit leads to a higher resulting flux density Φ_{Res} in the vicinity of the marker as depicted in Fig. 7 and explained in Eq. 2. The magnetic flux that passes through the turns of the coil is $\phi_{Coil} = \int B_1 \cdot \cos(\beta) dA$ where A is the area bounded by one turn of the coil and β the angle between the B_1 field and the orientation of the coil's axis of rotation. For the simulation, β is set to zero to obtain the best-case result.

Besides the increase of the magnetic field within and around the resonant marker, effects of superposition of the external field and the field of the coil can be observed as shown in Fig. 5. There is a $90°$ phase shift among the B_1 field used for excitation and the field generated by marker, shown in Fig. 5(c). Destructive and constructive superposition of the magnetic fields cause local minima and maxima within the resulting field. Fig. 6 describes the different regions of B field superposition. Fig. 7 depicts the resulting amplitude of the B_1 field in two points around the resonant marker and, in addition, the amplitude of the B_1 field without the resonant marker present.

Regarding Eq. 2, the resulting magnetic flux density ϕ_{Res}

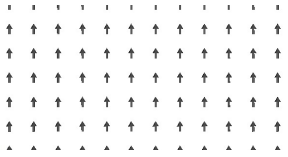

(a) Exciting B_1 field

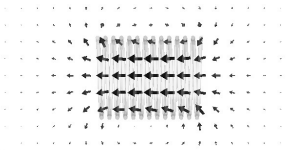

(b) Field from resonant marker resulting from B_1 field excitation

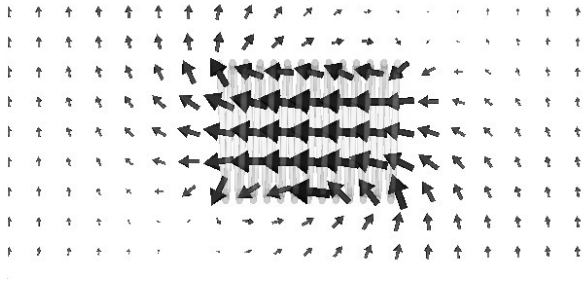

(c) Superposition of B_1 field and field from resonant marker

Fig. 5. Superposition of the B_1 field and the field generated by the resonant electric circuit due to the external excitation.

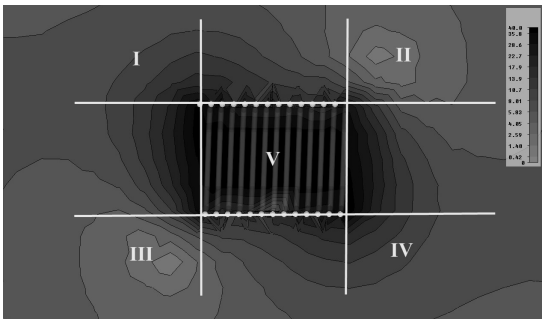

Fig. 6. Contour plot of the resulting B field vector plot from Fig. 5(c). Section I and IV: constructive B field superposition; section II and III: destructive B field superposition; section V: field within the resonant marker's coil.

within the resonant marker's coil depends linearly on the marker's Q factor. Fig. 8 depicts the B_x field within the center of the coil for $Q = 5$ and $Q = 10$ and, for comparison, the amplitude of the B_1 field without the resonant electric marker present. These results are confirmed by Eq. 2.

The sinc shaped signal used as one of the two excitation signals in the simulations entails a $180°$ phase shift of the B_1 field due to its zero crossing. This phase shift causes an destructive interference with the resonant marker's magnetic field generated from its stored energy. The shifted B_1 field interferes with the field from the marker and extenuates the circuits energy. This leads to more complex interference patterns as shown in Fig. 9.

IV. Results

A high signal intensity around the resonant marker has been observed during the experimental measurements as shown in Fig. 10. The usage of different excitation angles ranging from $1°$ to $90°$ results in different shapes of the corona surrounding the marker as shown in Fig. 10(a) and Fig. 10(b). The corona is rotated around its central point. By

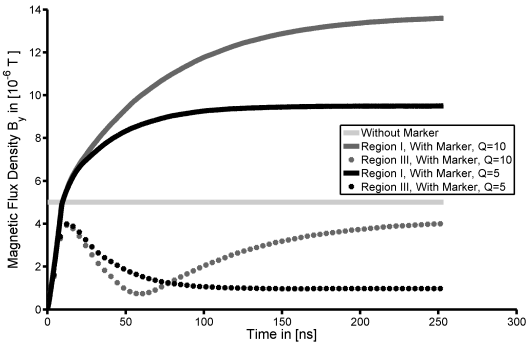

Fig. 7. Results of B field superposition for region I with constructive and region III with destructive superpostion in Fig. 5(c).

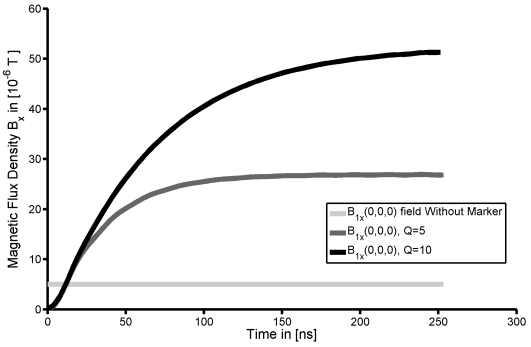

Fig. 8. B_{1x} field within the center of the resonant marker's coil for $Q = 5$ and $Q = 10$ and B_{1x} without the marker present.

(a) Excitation with a $sinc$ function, $\varphi(B_1) = 0°$

(b) Excitation with a $sinc$ function, $\varphi(B_1) = 90°$

Fig. 9. Magnetic field vectors around the resonant marker using a sinc shaped signal for the excitation of the B_1 field. Different regions with destructive superposition of the magnetic fields are observable.

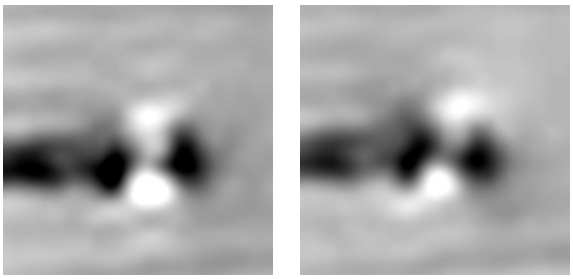

(a) Flip angle: $\alpha = 30°$

(b) Flip angle: $\alpha = 60°$

Fig. 10. Results from experimental measurements of the resonant marker using different flip angles. The symmetry axis of the corona is shifted within the MR image.

applying higher flip angles α, the corona undergoes a higher angle of rotation.

The simulation results from Fig. 5(c) and Fig. 9 show regions with constructive and destructive B field interferences. A constructive interference generates a higher local magnetic field intensity and vice versa. These interferences explain the asymmetric intensity distribution shown in Fig. 10.

As explained in Eq. 1, a higher B_1 field increases the flip angle α which leads, up to a certain point, to higher signal intensities. Regarding this fact, the external application of a very low flip angle, e.g. $\alpha \leq 1°$, could suppress the tissue's signal up to a certain amount but would still lead to a high signal within the vicinity of the marker.

V. Conclusion

The fabricated resonant electric marker was modeled regarding its geometrical and physical dimensions and simulated using a rotating magnetic field for the excitation of the resonant structure. The resulting magnetic field distribution shows regions of constructive and destructive magnetic field superposition.

The simulation results coincide with the findings from the experimental measurements. The fact that there is no symmetric distribution of the corona around the resonant marker can be explained by the resulting inhomogeneous distribution of the B_1 field around the resonant electric marker.

Medical devices like biopsy needles or catheters can be equipped with the resonant markers. This enhances the device's visibility within the MR image allowing a more precise placement of the instrument within the patient.

References

[1] J. L. Duerk, E. Y. Wong and J. S. Lewin, "A brief review of hardware for catheter tracking in magnetic resonance imaging", *MAGMA*, vol. 13, pp. 199-208, 2002.

[2] A. Glowinski, J. Kursch, G. Adam, A. Buecker, T.G. Noll and R.W.Guenther, "Device visualization for interventional MRI using local magnetic fields: basic theory and its application to catheter visualization", *IEEE Trans. Med. Imag.*, vol. 17, pp. 786-793, 1998.

[3] M. K. Konings, L. W. Bartels, C. F. van Swol and C.J.G. Bakker, "Development of an MR-safe tracking catheter with a laser-driven tip coil", *J Magn Reson Imaging*, vol. 13, pp. 131-135, 2001.

[4] C. Dumoulin, S. Souza and R. Darrow, "Real-time position monitoring of invasive devices using magnetic resonance", *Magn. Reson. Med.*, vol. 29, pp. 411-415, 1993.

[5] T. Kuehne, R. Fahrig and K. Butts, "Pair of resonant fiducial markers for localization of endovascular catheters at all catheter orientations", *J Magn Reson Imaging*, vol. 17, pp. 620-624, 2003.

[6] S. Weiss, T. Kuehne, F. Brinkert G. Krombach, M. Katoh, T. Schaeffter, R.W. Guenther and A. Buecker, "In vivo safe catheter visualization and slice tracking using an optically detunable resonant marker", *Magn Reson Med*, vol. 52, pp. 860-868, 2004.

[7] C.J. Bakker, R.M. Hoogeveen, W.F. Hurtak, J.J. van Vaals, M.A. Viergever and W. Mali, "MR-guided endovascular interventions: susceptibility-based catheter and near-real-time imaging technique", *Radiology*, vol. 202, pp. 273-276, 1997.

[8] K. Will, S. Schimpf, A. Brose F. Fischbach, J. Ricke, B. Schmidt and G. Rose, "Pre-tuned resonant marker for iMRI using aerosol deposition on polymer catheters", *Proc. SPIE*, vol. 7625, 2010.

[9] F. Fischbach, J. Bunke, M. Thormann, G. Gaffke, K. Jungnickel, J. Smink and Jens Ricke, "MR-Guided Freehand Biopsy of Liver Lesions With Fast Continuous Imaging Using a 1.0-T Open MRI Scanner: Experience in 50 Patients ", *Cardiovasc Intervent Radiol*, 2010.